

Silke Oellerich · Hainer Wackerbarth  
Peter Hildebrandt

## Conformational equilibria and dynamics of cytochrome *c* induced by binding of sodium dodecyl sulfate monomers and micelles

Received: 17 December 2002 / Revised: 7 April 2003 / Accepted: 7 April 2003 / Published online: 27 May 2003  
© EBSA 2003

**Abstract** Circular dichroism, nuclear magnetic resonance, electron paramagnetic resonance, UV-vis absorption, and resonance Raman (RR) spectroscopic techniques were employed to study protein and heme structural changes of cytochrome *c* (Cyt-*c*) induced by sodium dodecyl sulfate (SDS) monomers and micelles via hydrophobic and electrostatic interactions, respectively. Both modes of interactions cause the transition to the conformational state B2, which is implicated to be involved in the physiological processes of Cyt-*c*. At sub-micellar concentrations of SDS, specific binding of only ca. three SDS monomers, which is likely to occur at the hydrophobic peptide segment 81–85, is sufficient for a complete conversion to a B2 state in which Met80 is replaced by His33 (His26). These heme pocket structural changes are not linked to secondary structure changes of the protein brought about by nonspecific binding of SDS monomers in different regions of the protein. Upon binding of micelles, B2 high-spin species can also be stabilized by electrostatic interactions. In addition, the

micelle interaction domain is located on the front surface of Cyt-*c*, which includes a ring-like arrangement of lysine residues appropriate for binding one micelle. According to freeze-quench RR and stopped-flow experiments, state B2 is formed on the long millisecond timescale and reveals a complex dependence on the SDS concentration that can be interpreted in terms of competitive binding of monomers and micelles.

**Keywords** Cytochrome *c* · Electrostatic and hydrophobic interactions · Protein dynamics · Resonance Raman · Sodium dodecyl sulfate

### Introduction

Cytochrome *c* (Cyt-*c*) is an ubiquitous soluble heme protein that exerts a variety of physiological functions. Its role as an electron carrier in the respiratory chain of aerobic organisms has been known for decades and has inspired a large number of experimental studies (Scott and Mauk 1996). Nevertheless, there is still a considerable lack in the understanding on how the electron transfer to its partner proteins proceeds on a molecular level. Even much less is known about the second function of Cyt-*c* that has been discovered only recently: the involvement in the activation of an apoptotic pathway (Shi 2001). In this case, Cyt-*c* has to be transferred across the mitochondrial membrane into the cytosol, where it binds to the apoptosis protease activation factor-1 (Apaf-1). This complex activates procaspase-9 and thus initiates an enzymatic reaction cascade to cleave intracellular substrates that are essential for the living cell.

Using site-specifically mutated Cyt-*c* variants, it was possible to identify amino acids that are involved in binding to Apaf-1 (Yu et al. 2001). In the native form of Cyt-*c* in solution, these amino acid residues are distributed over the entire surface of the spherically shaped protein. It was suggested, therefore, that upon

S. Oellerich · H. Wackerbarth · P. Hildebrandt (✉)  
Max-Planck-Institut für Strahlenchemie,  
Stiftstrasse 34–36, 45470 Mulheim, Germany  
E-mail: hildebrandt@chem.tu-berlin.de  
Tel.: +49-30-31421419  
Fax: +49-30-31421122

P. Hildebrandt  
Instituto de Tecnológica Química e Biológica,  
Apartado 127, Av. da República, 2781-901  
Oeiras, Portugal

*Present address:* S. Oellerich  
Huygens Laboratory, Department of Biophysics,  
Leiden University, Niels Bohrweg 2,  
2333 CA Leiden, The Netherlands

*Present address:* H. Wackerbarth  
Biouorganisk Kemi, Danmarks Tekniske Universitet,  
Bygning 207, 2800 Lyngby, Denmark

*Present address:* P. Hildebrandt  
Max-Volmer-Laboratorium, Institut für Chemie,  
Technische Universität Berlin, Sekr. PC 14,  
Strasse des 17 Juni 135, 10623 Berlin, Germany

complex formation, Cyt-*c* is partly encapsulated by the polypeptide chain of Apaf-1. However, it may be that structural changes are induced in apoptotic Cyt-*c* such that these amino acids, which are originally largely separated from each other, are brought into a more confined domain. Evidence for structural changes of Cyt-*c* in apoptosis has been provided by Jemmerson et al. (1999). These authors have shown that apoptotic Cyt-*c* binds to antibodies which do not recognize the native protein but instead Cyt-*c* bound to membranes. The findings suggest that the underlying structural changes in apoptotic Cyt-*c* are related to those induced in complexes with phospholipid vesicles that include alterations of the tertiary structure and the heme pocket (Hildebrandt et al. 1990; Muga et al. 1991; Spooner and Watts 1991; Heimburg and Marsh 1993; Pinheiro 1994; Döpner et al. 1999; Oellerich et al. 2002). In such complexes, new conformational states, denoted as B2, are formed which are structurally different from the native Cyt-*c* and are, therefore, also denoted as non-native states. A common characteristic of the non-native B2 states is the dissociation of the axial Met80 ligand from the heme iron (Oellerich et al. 2002). This coordination site remains either vacant (five-coordinated high-spin, 5cHS) or is occupied by His33 (His26) (six-coordinated low-spin, 6cLS), as concluded from a comparative resonance Raman (RR) and electron paramagnetic resonance (EPR) spectroscopic study.

Complex formation of Cyt-*c* with the natural redox partner cytochrome *c* oxidase (CcO) involves the lysine-rich domain around the exposed heme edge (Pettigrew and Moore 1987). These residues are located in a ring-like arrangement on the front surface of Cyt-*c* and no significant structural adjustments are required to match with the distribution of complementarily charged residues in the binding domains of the partner protein and to establish a hydrophobic contact region (Ferguson-Miller and Babcock 1996; Roberts and Pique 1999) that is essential for the electron transfer (Witt et al. 1998). Nevertheless, at least in the case of CcO, formation of the fully oxidized complex leads to an equilibrium between the native state B1 to the conformational state B2 (Döpner et al. 1999). It has been suggested that this conformational transition may be of functional relevance for the physiological redox process (Döpner et al. 1999; Wackerbarth et al. 2001).

Thus, complex formation with the partner proteins in electron transfer chains and apoptotic reaction cascades appears to be associated with different binding domains and structural requirements of Cyt-*c*, although there may be similarities in the putative structural response of Cyt-*c*. Clearly, a more detailed knowledge about these conformational changes is required for understanding both physiological functions of Cyt-*c* on a molecular level.

In this respect, the analysis of Cyt-*c*'s interactions with self-assembled aggregates of amphiphilic molecules are of particular interest in view of the obvious

similarities between membrane-induced structural changes and those implicated to be involved in the physiological processes. Sodium dodecyl sulfate (SDS) is spectroscopically silent for various techniques and has been used previously for studying the unfolding processes of Cyt-*c* (Das et al. 1998; Gębicka and Gębicki 1999; Otzen and Oliveberg 2002). Moreover, we have recently shown that SDS promotes the conversion to the same conformational state (B2) as binding to liposomes or CcO (Döpner et al. 1999; Oellerich et al. 2002). Thus, SDS offers a convenient model system for a detailed study of the structure and the formation of the putatively functionally relevant state B2. As an additional advantage, SDS allows varying the interplay between electrostatic and hydrophobic interactions in a systematic manner and thereby may give deeper insight into the parameters that control the conformational transitions. In this work, we have employed circular dichroism (CD), nuclear magnetic resonance (NMR), UV-vis absorption, RR, and EPR spectroscopy as well as stopped-flow and freeze-quench techniques to analyse the structure as well as the mechanism and dynamics of the formation of this conformational state.

---

## Material and methods

### Materials

Horse heart cytochrome *c* (Sigma, type VI) was dissolved in 50 mM phosphate buffer or 1 mM 4-(2-hydroxyethyl)piperazine-1-ethanesulfonic acid (HEPES) buffer at pH 7. All experiments were carried out with oxidized Cyt-*c*. For UV-vis absorption, CD, and RR spectroscopy at ambient temperature the protein concentration was 10, 15, and 15  $\mu\text{M}$ , respectively. For stopped-flow measurements the concentration was set to 2.5  $\mu\text{M}$  and to 100  $\mu\text{M}$  for low-temperature and freeze-quench RR spectroscopy, unless noted otherwise. EPR and NMR spectroscopic experiments were carried out with 1 mM Cyt-*c*.

### UV-vis absorption spectroscopy

UV-vis absorption spectra were recorded on a Unicam UV2 spectrophotometer with a spectral resolution of 0.5  $\text{cm}^{-1}$ , a bandwidth of 4 nm, and a scan speed of 600 nm/min. The path length of the measuring cell was 10 mm for all experiments.

### Resonance Raman spectroscopy

RR spectra were measured at ambient temperature with the 413-nm excitation line of a  $\text{Kr}^+$  laser (Coherent Innova 302) using a spectrograph (U1000, ISA) equipped with a liquid nitrogen cooled CCD camera. The spectral resolution was 4  $\text{cm}^{-1}$  (Wackerbarth et al. 1999). The incident laser beam (40 mW) was focused on the sample that was placed in a rotating cell. All RR measurements were repeated several times under the same conditions to ensure reproducibility. To improve the signal-to-noise ratio, the individual spectra were added if no spectral differences were noted. Spectral contributions of SDS were subtracted and the structureless background was removed by polynomial subtraction. The resulting spectra were analysed by a component analysis (Döpner et al. 1996).

### Low-temperature and freeze-quench resonance Raman spectroscopy

Freeze-quenched samples were prepared with a BioLogic MPS-52 Mixcon apparatus as described previously (Oellerich et al. 2000). Short EPR tubes containing the freeze-quenched samples were fixed to a home-built sample holder and placed into a cryostat (Cryovac) that allowed temperature control between 77 and 313 K. The power of the incident laser beam focused on the sample was less than 20 mW. Scattered light was collected in a 135° geometry. The signal-to-noise ratio was improved by adding up individual spectra that were recorded at 133 K. Some spectra contained contributions from residual isopentane, which were removed by subtraction of a spectrum of pure isopentane measured under the same conditions. The structureless background was removed by polynomial subtraction and the resulting spectra were subjected to a component analysis.

### Circular dichroism spectroscopy

Spectra were recorded at ambient temperature on a JASCO J-715 spectropolarimeter. Far-UV CD spectra (190–260 nm) were measured using a quartz cell of 1 mm path length, whereas for near-UV and Soret CD spectra (250–500 nm) a quartz cell of 10 mm path length was employed. Four scans were averaged per spectrum. The spectral resolution was 0.5 nm. Furthermore, a bandwidth of 1 nm and a response time of 1 s were typically used.

### <sup>1</sup>H NMR spectroscopy

<sup>1</sup>H NMR spectra of the samples in 50 mM deuterated phosphate buffer in D<sub>2</sub>O (pD 7, uncorrected reading) were recorded on a Bruker DRX 400 MHz spectrometer.

### Electron paramagnetic resonance spectroscopy

X-band EPR spectra (9.6 GHz) were measured with an ESP 300E spectrometer (Bruker) equipped with an ER 041 XK-D microwave bridge (Bruker) and a helium flow cryostat (ESR 910; Oxford Instruments) to maintain a temperature of 10 K. The modulation frequency was set to 100 kHz.

### UV-vis absorption stopped-flow spectroscopy

UV-vis absorption stopped-flow experiments were carried out in the temperature range between 11.5 and 34.4 °C using a home-built set-up. The global analysis of the transient spectra was performed using a self-written program (R. Schumacher, MPI für Strahlenchemie, Mülheim, Germany).

## Results

### Spectroscopic characterization of the SDS-induced structural changes of Cyt-*c*

Far-UV CD spectra of Cyt-*c*, measured as a function of the SDS concentration, reveal an intensity decrease of the 220 nm dichroic band of about 25% and thus a loss of  $\alpha$ -helical structure of the Cyt-*c*. These changes are essentially completed at a SDS concentration of 0.9 mM (Fig. 1). A further increase of the SDS concentration up to 2 mM does not result in a further loss of  $\alpha$ -helical

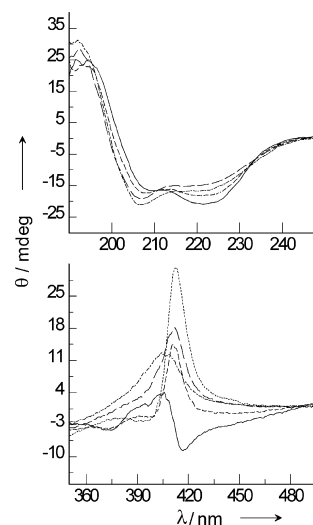


**Fig. 1** CD spectra of 15  $\mu$ M Cyt-*c* in 50 mM phosphate buffer (pH 7). Far-UV (*top*) and near-UV/Soret (*bottom*) CD spectra of Cyt-*c* were obtained before and after addition of SDS at ambient temperature. No SDS: *full line*; 0.5 mM SDS: *dashed line*; 1.2 mM SDS (only in the bottom panel): *dotted line*; 2.0 mM SDS: *long dashed line*; 50 mM SDS: *dash-dot line*

structure, while the addition of SDS at concentrations above 2 mM leads to an intensity increase of the 220 nm dichroic band. Interference of the CD signals by concentration-dependent changes of the light scattering can be ruled out since in the absence of Cyt-*c* the CD spectra were found to be identical over the entire SDS concentration range studied here. The near-UV CD spectra reveal a different behavior inasmuch as the minima at 282 and 288 nm, both sensitive indicators for a tight packing of the heme pocket (Davies et al. 1993), have largely disappeared already at a SDS concentration of ca. 0.9 mM but do not recover upon further increase of surfactant concentration. Also the 417-nm minimum in the Soret band region (Fig. 1) disappears at concentrations below 0.9 mM. This spectral change is accompanied by intensification and a 6-nm upshift of the 406 nm maximum to 412 nm. A further increase of the SDS concentration above 1.2 mM results in an intensity decrease and broadening of the positive dichroic band, the maximum of which is then shifted to 405 nm.

In the <sup>1</sup>H NMR spectra, SDS-induced tertiary structural changes are reflected by a concentration of proton resonances between 6.5 and 7.5 ppm (Fig. 2). This phenomenon was previously observed by de Jongh et al. (1992) upon Cyt-*c* binding to mixed dodecylphosphocholine/dodecylphosphoglycol micelles and ascribed to a relaxation of the native tertiary protein structure. Furthermore, large paramagnetic shifts of the peaks are observed at high SDS concentrations (Fig. 2), indicating the formation of a ferric high-spin (HS) species.

In the UV-vis absorption spectra, the 695-nm band, which is indicative for the coordination of the native Met80 heme ligand, disappears at SDS concentrations <1 mM (Fig. 3), whereas above 2 mM SDS an

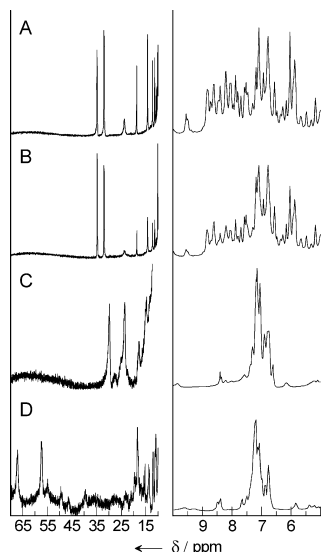


**Fig. 2**  $^1\text{H}$  NMR spectra of Cyt-*c* in SDS measured at 27 °C in 50 mM deuterated phosphate buffer (pH 7) in the absence of SDS (A), and in the presence of (B) 3.7 mM, (C) 25 mM, and (D) 85 mM SDS. The intensity scale in the region between 70 and 10 ppm is enlarged by a factor of (A) 5, (B) 2, and (C, D) 50 compared to the region between 10 and 5 ppm. The protein concentration was 1 mM in all  $^1\text{H}$  NMR experiments

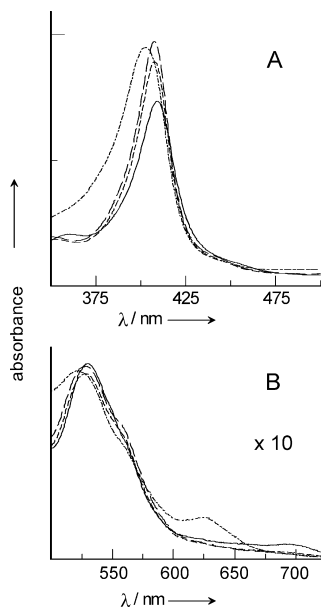


**Fig. 3** UV-vis absorption spectra of Cyt-*c* in 50 mM phosphate buffer (pH 7.0) before and after addition of SDS. The Soret band and visible regions are shown in A and B, respectively. No SDS: full line; 0.7 mM SDS: dashed line; 2.0 mM SDS: long dashed line; 100 mM SDS: dash-dot line

absorption band at 625 nm is observed that is characteristic for a ferric HS species (Makinen and Churg 1983). The increase of the 625-nm band is accompanied by an intensity decrease and a blue shift of the Q-band and an increased absorption at 490 nm. The Soret absorption band displays a slight blue shift (407 nm)

below 2 mM SDS and shifts down further to 401 nm at an SDS concentration of 500 mM.

The EPR spectrum of the native ferric Cyt-*c* (Fig. 4) exclusively displays LS signals with  $g_1$ ,  $g_2$ , and  $g_3$  values of 3.03, 2.25, and 1.18, respectively, which are shifted to 2.93, 2.25, and 1.5 upon addition of SDS. With increasing SDS concentration the intensity of the LS signals decrease in favor of a signal characteristic for a HS species ( $g_{\perp} = 5.76$ ). The variation of the SDS concentration (50–500 mM) leaves the  $g$  values unchanged.

In the RR spectra, those conformational states of Cyt-*c* can be distinguished that differ by their heme structures, that is the geometry of the porphyrin, the spin and ligation states, and the kind of axial ligands (Kitagawa and Ozaki 1987; Parthasarathi et al. 1987; Alden et al. 1989; Smith 1993). In aqueous solution at pH 7.0 the heme iron of native Cyt-*c* is axially coordinated by His18 and Met80, leading to a 6cLS configuration. This configuration is reflected by the characteristic frequencies of the RR marker bands  $\nu_4$ ,  $\nu_3$ ,  $\nu_2$ , and  $\nu_{10}$ , which for the ferric form are at 1372, 1502, 1584, and 1635  $\text{cm}^{-1}$ , respectively (spectrum not shown). Addition of up to 2 mM SDS leads to distinct shifts of the RR marker bands to higher frequencies, while remaining in the range characteristic of a 6cLS species. Furthermore, the  $\nu_{11}$  mode of native ferric Cyt-*c* at 1560  $\text{cm}^{-1}$  disappears and the  $\nu_{10}$  mode suffers a substantial intensity decrease (Fig. 5).

Upon increasing the SDS concentration above 2 mM, a broadening of the band at ca. 1506  $\text{cm}^{-1}$  ( $\nu_3$ ) and a distinct shoulder at the low-frequency side of the 1588- $\text{cm}^{-1}$  peak ( $\nu_2$ ) are observed (Fig. 5), indicating the formation of one or more additional non-native species.

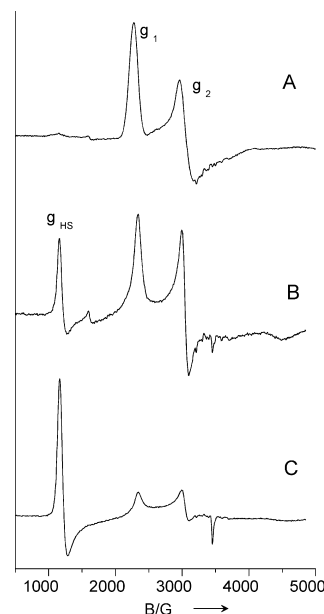


**Fig. 4** X-band EPR spectra of Cyt-*c* measured at 10 K (A) in the absence of SDS and (B) in the presence of 100 mM and (C) 500 mM SDS. The protein concentration was 1 mM and a 50 mM phosphate buffer (pH 7.0) was used

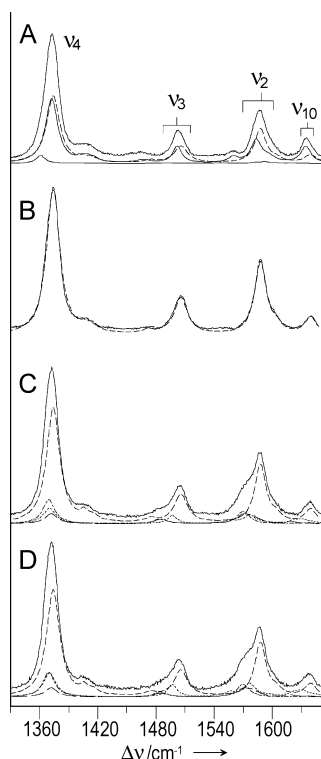


**Fig. 5** RR spectra of Cyt-*c* in the marker band region between 1300 and 1650  $\text{cm}^{-1}$ . The spectra were measured with a 413-nm excitation at ambient temperature from 15  $\mu\text{M}$  Cyt-*c* solution in 50 mM phosphate buffer (pH 7.0) containing (A) 0.5 mM, (B), 2.0 mM, (C) 10 mM, and (D) 200 mM SDS. The component spectra of the various heme configurations are indicated by different line types: B1[6cLS]: *full line*; B2[6cLS]: *dashed line*; B2[6cHS(1)]: *dash-dot line*; B2[6cHS(2)]: *long dashed line*; and B2[5cHS]: *short dashed line*

Subtracting the RR spectrum measured in the presence of 2 mM SDS (corresponding to the “pure” non-native 6cLS species) from RR spectra obtained at higher SDS concentrations yields difference spectra that display bands indicative for ferric HS species. In fact, a global analysis of the RR has revealed that SDS induces four non-native ferric species that are a 6cLS, a 5cHS, and two 6cHS forms, denoted as B2[6cLS], B2[5cHS],

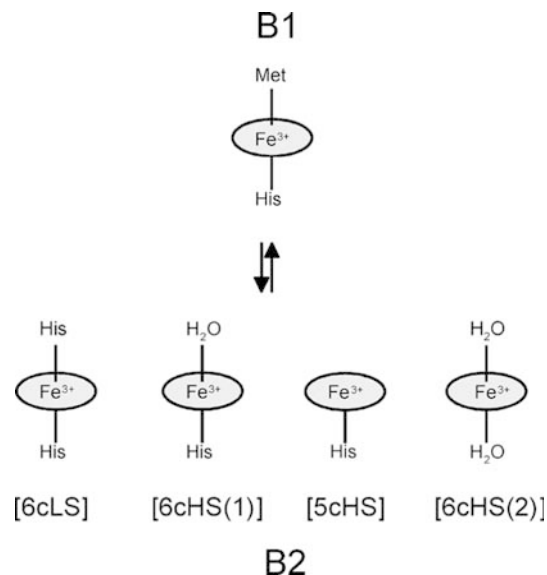


**Fig. 6** Schematic representation of the native (B1) and SDS-induced (B2) ferric heme configurations

B2[6cHS(1)], and B2[6cHS(2)], respectively (Oellerich 2001; Oellerich et al. 2002). As shown previously, in all of these B2 species the Met80 ligand of native Cyt-*c*, denoted as B1[6cLS], is removed from the heme iron and either replaced by His33 (His26) or a water molecule in B2[6cLS] and B2[6cHS(1)], respectively (Oellerich et al. 2002). In B2[5cHS] this coordination site remains vacant whereas in B2[6cHS(2)] both axial ligands are replaced by water molecules (Fig. 6).

Quantitative analysis of the heme structural changes at ambient temperature

The RR spectral parameters of the various conformational states of Cyt-*c* (Table 1) define the respective component spectra that constitute the basis for the quantitative analysis of the RR experiments. Simulating the measured RR spectra by these component spectra

**Table 1** Frequencies and relative intensities (in parentheses) of RR marker bands of the various states of Cyt-*c* formed upon binding to SDS micelles and monomers at ambient and low temperature

Species	Axial ligands	$T$ (K)	Modes			
			$\nu_4$ ( $\text{cm}^{-1}$ )	$\nu_3$ ( $\text{cm}^{-1}$ )	$\nu_2$ ( $\text{cm}^{-1}$ )	$\nu_{10}$ ( $\text{cm}^{-1}$ )
B1[6cLS]	His/Met	293	1372.5 (1.00)	1501.9 (0.26)	1583.6 (0.35)	1634.7 (0.25)
		133	1374.8 (1.00)	1505.3 (0.27)	1586.5 (0.38)	1638.5 (0.36)
B2[6cLS]	His/His	293	1374.1 (1.00)	1505.8 (0.25)	1587.8 (0.50)	1639.6 (0.12)
		133	1376.9 (1.00)	1509.9 (0.21)	1591.5 (0.55)	1642.1 (0.14)
B2[5cHS]	His/-	293	1370.3 (1.00)	1496.9 (0.52)	1576.7 (0.55)	1622.5 (0.16)
		133	1371.0 (1.00)	1496.0 (0.59)	1577.0 (0.41)	1622.0 (0.16)
B2[HS] <sup>fa</sup>	His/-	133	1369.2 (1.00)	1493.2 (0.34)	1579.1 (0.86)	1631.7 (0.07)
B2[6cHS(1)]	His/H <sub>2</sub> O	293	1369.5 (1.0)	1484.7 (0.20)	1569.1 (0.44)	n.d.
A[6cLS]		133	1376.1 (1.00)	1507.6 (0.39)	1590.9 (0.53)	1641.1 (0.20)
B2[6cHS(2)]	H <sub>2</sub> O/H <sub>2</sub> O	293	1372.0 (1.00)	1483.9 (0.40)	1570.3 (0.79)	1619.4 (0.20)
		133	1367.2 (1.00)	1485.7 (0.26)	1579.0 (0.78)	1634.0 (0.12)

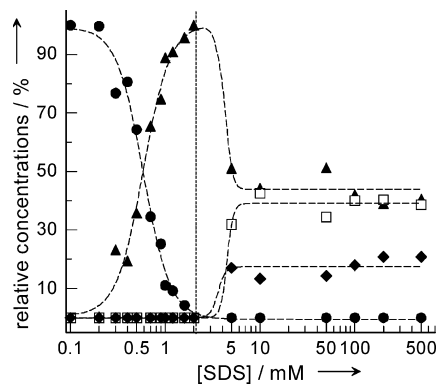


**Fig. 7** Relative concentrations of the Cyt-*c* species at ambient temperature in 50 mM phosphate buffer (pH 7) as a function of the SDS concentration. The different Cyt-*c* species are represented by the following symbols: B1[6cLS]: *solid circles*; B2[6cLS]: *solid triangles*; and B2[5cHS]: *solid diamonds*. The relative concentrations of the B2[6cHS(1)] and B2[6cHS(2)] species are summed up to B2[6cHS] and expressed by *open squares*. The *dotted lines* illustrate the concentration curves, while the *vertical dashed line* marks the CMC. The results of the quantitative analysis are based on the component analysis of the RR spectra measured at various SDS concentrations in 50 mM phosphate buffer. The protein concentration was 15  $\mu\text{M}$ . Further details are given in the text

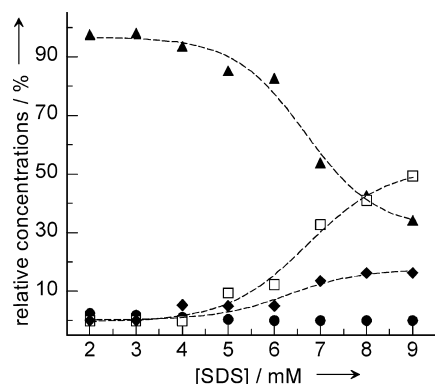


**Fig. 8** Relative concentrations of the Cyt-*c* species at ambient temperature in 1 mM HEPES buffer (pH 7) as a function of the SDS concentration. The different Cyt-*c* species are represented by the following symbols: B1[6cLS]: *solid circles*; B2[6cLS]: *solid triangles*; and B2[5cHS]: *solid diamonds*. The relative concentrations of the B2[6cHS(1)] and B2[6cHS(2)] species are summed up to B2[6cHS] and expressed by *open squares*. The *dotted lines* illustrate the concentration curves. The results of the quantitative analysis are based on the component analysis of the RR spectra measured at various SDS concentrations in 1 mM HEPES buffer. The protein concentration was 15  $\mu\text{M}$ . Further details are given in the text

yields the relative spectral contributions of the various species, which are subsequently converted into relative concentrations using the reciprocal relative RR cross-sections determined previously (Oellerich 2001; Oellerich et al. 2002). The component analysis was applied to RR spectra measured from Cyt-*c*/SDS solutions containing HEPES and phosphate buffer. In Figs. 7, 8, and 9 the relative contributions of both 6cHS species are combined for the clarity of the representation.

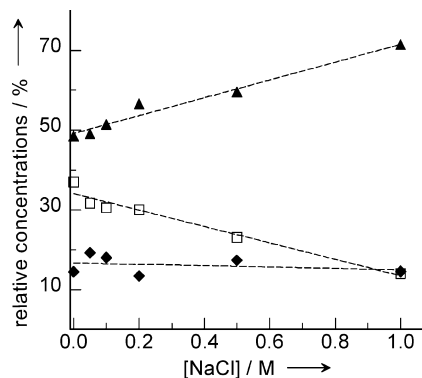


**Fig. 9** Relative concentrations of the SDS-induced Cyt-*c* species at ambient temperature in 20 mM SDS solutions (50 mM phosphate buffer, pH 7) as a function of NaCl concentration. The different Cyt-*c* species are represented by the following symbols: B2[6cLS]: *solid triangles*; B2[5cHS]: *solid diamonds*. The relative concentrations of the B2[6cHS(1)] and B2[6cHS(2)] species are summed up to B2[6cHS] and expressed by *open squares*. The *dotted lines* illustrate the concentration curves. The results of the quantitative analysis are based on the component analysis of the RR spectra measured in 20 mM solution at different NaCl concentrations. The protein concentration was 15  $\mu\text{M}$ . Further details are given in the text

For solutions buffered with 50 mM phosphate buffer (Fig. 7), the only non-native Cyt-*c* species that is formed up to an SDS concentration of ca. 2 mM is the bis-His coordinated B2[6cLS] state, the contribution of which steadily increases to 95% at the expense of the native B1[6cLS] form. Above an SDS concentration of 2 mM, which corresponds to the critical micelle concentration (CMC) of SDS in the solution containing 50 mM phosphate buffer at pH 7 (Takeda et al. 1985; Yoshimura 1988), HS species are also formed until at ca. 10 mM SDS the distribution among the various non-native species, that is 40% B2[6cLS], 40% B2[6cHS(1)] + B2[6cHS(2)], and 20% B2[5cHS], remains constant (Fig. 7).

In solutions containing 1 mM HEPES buffer, the CMC of SDS is increased to ca. 7 mM (Emerson and Holtzer 1967; Reynolds and Tanford 1970). In this case, the onset of the formation of HS species is observed at distinctly higher SDS concentrations (ca. 5 mM), but the relative concentration of the 6cHS forms at ca. 9 mM is higher (50%) than in the presence of 50 mM phosphate (Fig. 8). Conversely, in solutions containing 20 mM SDS and 50 mM phosphate buffer the relative contributions of both B2[6cHS(1)] and B2[6cHS(2)] decrease in a largely parallel manner upon addition of NaCl such that in the presence of 1 M NaCl their total contribution is only ca. 30% (Fig. 9). This tendency parallels the decrease of the CMC that results from the increase of the ionic strength (Emerson and Holtzer 1967; Reynolds and Tanford 1970). On the other hand, the content of B2[5cHS] remains essentially constant.

The results obtained from the RR experiments with solutions of different buffers and ionic strengths are in line with the qualitative analysis of the UV-vis absorption spectra that allow monitoring the formation

of HS species on the basis of the 625-nm absorption band (vide infra).

#### Quantitative analysis of the heme structural changes at low temperature

Although the spin and ligation state of native ferric Cyt-*c*, B1[6cLS], is not altered upon lowering the temperature to 133 K, the RR marker bands  $\nu_4$ ,  $\nu_3$ ,  $\nu_2$ , and  $\nu_{10}$  exhibit frequency upshifts to 1375, 1505, 1586.5, and 1638.5  $\text{cm}^{-1}$ , respectively, whereas the relative intensities remain largely unchanged (Table 1) (Cartling 1983). Comparable frequency shifts and also only small intensity variations were noted for B2[6cLS], so that for these two species the low-temperature correction of the component spectra was straightforward. This is also true for the B2[5cHS], which exhibits even smaller temperature-dependent frequency shifts than the LS forms. For ferric 6cHS hemes, spin pairing may occur at low temperature, as was also observed for the His/aqua-coordinated ferric Cyt-*c* that is formed in aqueous solution at low pH and high ionic strength (Oellerich et al. 2002). In this so-called A-state, the 6cHS configuration that displays essentially the same RR spectra as B2[6cHS(1)] is converted to a 6cLS form denoted as A[6cLS] upon lowering the temperature to 133 K. In fact, a good global analysis of the low-temperature RR spectra of Cyt-*c* in SDS solutions measured in this work can be achieved on the basis of the low-temperature component spectra of B1[6cLS], B2[6cLS], A[6cLS], and B2[5cHS] as well as of a 6cHS form (Oellerich et al. 2002). This latter species is ascribed to B2[6cHS(2)] since the His/aqua-coordinated HS form is converted to a LS configuration.

The component analysis of the low-temperature RR spectra of Cyt-*c* ([Cyt-*c*] = 100  $\mu\text{M}$ ) in SDS solutions containing 50 mM phosphate buffer (no additional salt) provide a similar, albeit not identical, picture as the experiments at ambient temperature, that is, the increase of B2[6cLS] at the expense of B1[6cLS] up to a SDS concentration of ca. 2 mM. However, the limiting value of the B2[6cLS] concentration is lower by 10% than in the experiments at 293 K. Above 2 mM, the B2[5cHS], B2[6cHS(2)], and the A[6cLS] states increase with increasing SDS concentrations. The limiting concentrations of A[6cLS] is only 50% of the value determined for its counterpart at ambient temperature {B2[6cHS(1)]}, whereas that of B2[5cHS] is essentially the same.

#### Freeze-quench resonance Raman spectroscopy

Applying the set of component spectra derived from the low-temperature experiments, in which the samples were slowly cooled to 133 K, to the analysis of the RR spectra of samples obtained by rapid freeze-quenching did not result in a consistent global fit. Whereas at low SDS concentrations a satisfactory simulation was achieved,

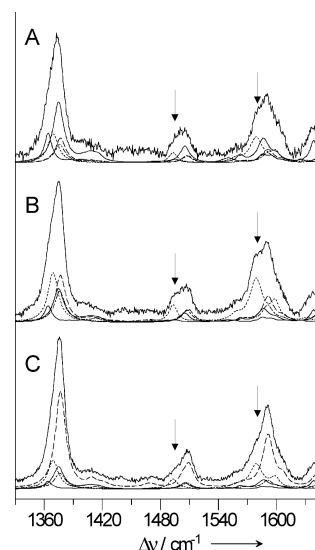


**Fig. 10** Low-temperature freeze-quench RR spectra of Cyt-*c* in the marker band region between 1300 and 1650  $\text{cm}^{-1}$ . All spectra were measured at  $-140$  °C with 413-nm excitation. The protein and SDS concentration were 100  $\mu\text{M}$  and 150 mM, respectively. The samples were prepared after reaction times of (A) 33 ms, (B) 88 ms, and (C) 9 s. The component spectra of the various heme configurations are indicated by different line types: B1<sup>T</sup>[6cLS]: full line; B2<sup>T</sup>[6cLS]: dashed line; A<sup>T</sup>[6cLS]: dash-dot line; and B2[HS]<sup>fq</sup>: short dashed line. Further details are given in the text

the quality of the fits was not acceptable for samples of high SDS concentrations, corresponding to relatively high contributions of HS species. In fact, the most severe deviations were noted in the spectral regions that are dominated by bands expected for HS configurations ( $\nu_3$ , 1480–1495  $\text{cm}^{-1}$ ;  $\nu_2$ , 1560–1575  $\text{cm}^{-1}$ ), indicating structural and thus RR spectroscopic differences of the HS forms in samples obtained by rapid freeze-quenching and slow cooling. A good global fit to all freeze-quench RR spectra could be achieved upon replacing the component spectra of B2[5cHS] and B2[6cHS(2)] by a component spectrum of just one HS species, denoted as B2[HS]<sup>fq</sup>. The spectral parameters of B2[HS]<sup>fq</sup> are closer to those characteristic of a 5cHS rather than a 6cHS configuration (Table 1). Thus, we assume that this component spectrum largely represents a 5cHS species in which the heme pocket structure is not fully relaxed.

Figure 10 shows a selection of RR spectra of freeze-quenched samples obtained at different reaction times ([SDS] = 150 mM). Comparison of the spectra obtained at 33 and 88 ms indicates an increase of B2[HS]<sup>fq</sup> and A[6cLS] at the expense of B1[6cLS], as is reflected by the increase of bands at ca. 1490 and 1575  $\text{cm}^{-1}$  (marked by arrows). At longer reaction times, the contribution of this species decreases again, whereas that of B2[6cLS] increases.

The freeze-quench RR experiments were carried out with samples containing 5, 10, and 150 mM SDS. For the quantitative evaluation of the data derived from the component analysis, the relative contributions of B2[HS]<sup>fq</sup> were combined with those of A[6cLS] (vide

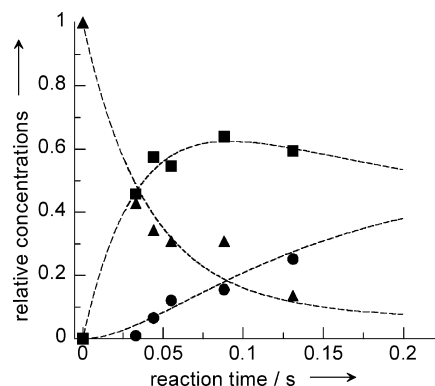
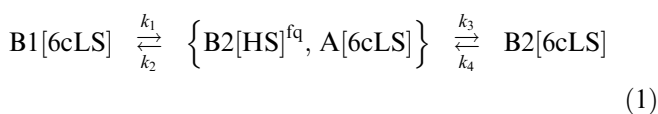


**Fig. 11** Relative concentrations of the Cyt-*c* species as a function of reaction time with 150 mM SDS. The relative contributions of the different Cyt-*c* species are represented by *solid diamonds* and *solid circles* for B1[6cLS] and B2[6cLS], respectively. The relative concentrations of B2[HS]<sup>fq</sup> and A[6cLS] species are summed up to B2[HS] and denoted by *solid squares*. Relative contributions from the reduced HS from of B2, which do not exceed 2.4%, are not shown in the graph for the sake of clarity of presentation. The *dotted lines* represent the result of the simulation based on a two-step reaction mechanism. The results of the quantitative analysis are based on the component analysis of the freeze-quench RR spectra measured at  $-140\text{ }^{\circ}\text{C}$ . Further details are given in the text

infra) (Fig. 11). The underlying assumption is that the transition between the mono-His coordinated B2[HS]<sup>fq</sup> and the His/aqua coordinated A[6cLS] is fast on the timescale of the experiments inasmuch as it most likely requires just the movement of a water molecule towards the heme rather than extended structural changes of the heme pocket. Within the accuracy of the experiments and the spectra analysis, there is no indication for a separated time evolution of both species. Consequently, the minimal kinetic scheme is given by:



with:

$$K_{\text{AB}} = \frac{[\text{B1}(6\text{cLS})]}{([\text{B2}(\text{HS})^{\text{fq}}] + [\text{A}(6\text{cLS})])} = \frac{k_2}{k_1} \quad (2)$$

and:

$$K_{\text{AB}} = \frac{([\text{B2}(\text{HS})^{\text{fq}}] + [\text{A}(6\text{cLS})])}{[\text{B2}(6\text{cLS})]} = \frac{k_4}{k_3} \quad (3)$$

defining the equilibrium constants that were determined from the RR spectra measured under stationary conditions at low temperature. Thus, the kinetic model includes only two independent variables (rate constants) that were fitted to the experimental data. For all series of measurements a satisfactory description of the time-dependent concentration changes was achieved, as illustrated, for example, for the reaction of Cyt-*c* in 150 mM SDS solution (Fig. 11). The rate constants that

**Table 2** Equilibrium and rate constants for the reaction of Cyt-*c* with SDS obtained from freeze-quench experiments<sup>a</sup>

[SDS] (mM)	5	10	150
[SDS] <sub>micl</sub> /[Cyt]	0.5	1.4	25
$K_{\text{A/B}}$	0.22	0.18	0.12
$K_{\text{B/C}}$	0.30	0.40	0.79
$k_1$ (s <sup>-1</sup> )	12	13	23
$k_2$ (s <sup>-1</sup> )	3	2	3
$k_3$ (s <sup>-1</sup> )	43	20	5
$k_4$ (s <sup>-1</sup> )	13	8	4

<sup>a</sup>The constants refer to Eqs. (1, 2, 3). “A”, “B”, and “C” denote the states B1[6cLS], (B2[HS]<sup>fq</sup>, A[6cLS]), and B2[6cLS], respectively. The values for  $k_1$  are considered to be lower limits

are listed in Table 2 show that raising the SDS concentration causes an increase of  $k_1$ , whereas  $k_3$  and  $k_4$  decrease and  $k_2$  remains constant.

### UV-vis stopped-flow experiments

The characteristic UV-vis absorption changes of Cyt-*c* that are induced by interactions with SDS can be used to monitor the conformational dynamics in stopped-flow experiments. These changes are illustrated by the difference spectra obtained for increasing reaction times of Cyt-*c* with 10 mM SDS. With increasing reaction time, the positive and negative peaks shift from 395 to 399 nm

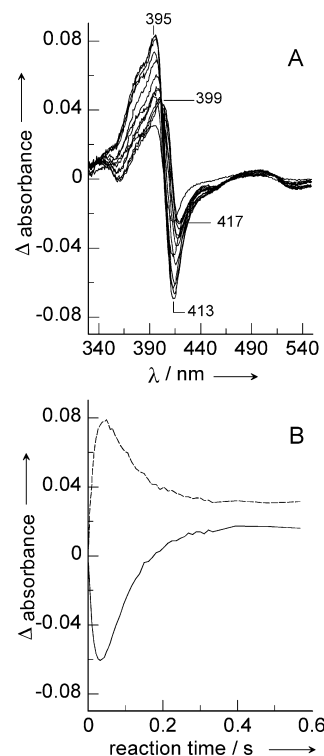


**Fig. 12** UV-vis stopped-flow absorption measurements of the reaction of 2.5  $\mu\text{M}$  Cyt-*c* in 50 mM phosphate buffer (pH 7.0) with 10 mM SDS ( $T=25\text{ }^{\circ}\text{C}$ ). Difference spectra are shown in **A** whereas absorption transients at 390 nm (*dashed line; top*) and 410 nm (*solid line; bottom*) are displayed in **B**



**Table 3** Rate constants (in s<sup>-1</sup>) of the reaction of Cyt-*c* with SDS determined from stopped-flow experiments<sup>a</sup>

[SDS] (mM)	[SDS] <sub>mic</sub> /[Cyt]	11.5 °C		17 °C		21.9 °C		25.7 °C		30.0 °C		34.4 °C	
		<i>k</i> <sub>obs,1</sub>	<i>k</i> <sub>obs,2</sub>	<i>k</i> <sub>obs,1</sub>	<i>k</i> <sub>obs,2</sub>	<i>k</i> <sub>obs,1</sub>	<i>k</i> <sub>obs,2</sub>	<i>k</i> <sub>obs,1</sub>	<i>k</i> <sub>obs,2</sub>	<i>k</i> <sub>obs,1</sub>	<i>k</i> <sub>obs,2</sub>	<i>k</i> <sub>obs,1</sub>	<i>k</i> <sub>obs,2</sub>
2.5	5	8.3	1.6	14.9	3.5	26.5	7.7	40.1	13.3	62.5	25.2	107	44.8
5	21	9.4	1.5	17.4	3.6	29.9	7.8	46.5	13.1	75.2	23.7	122.8	44.3
7.5	38	10.4	1.5	18.8	3.4	33.1	7.3	51.8	12.5	81.0	23.1	139.4	41.7
10	55	11.4	1.4	19.9	3.9	33.5	7.1	53.8	12.2	89.2	22.4	156.6	39.6
15	88	13.9	1.2	22.2	3.2	39.2	7.0	60.1	11.8	99.2	21.7	184.3	38.1
20	120	–	–	23.5	3.3	41.3	6.9	64	11.9	105.2	21.1	–	–

<sup>a</sup>The rate constants refer to Eq. (4). “A” denotes the native state B1[6cLS], whereas “B” and “C” refer to mixtures of predominantly B2[HS] and B2[6cLS] species, respectively

and from 413 to 417 nm, respectively (Fig. 12A). The absorption transients at 390 and 410 nm show the time course of the underlying processes (Fig. 12B).

The global analysis was carried out on the basis of two exponentials and a linear drift. The two rate constants, *k*<sub>obs,1</sub> and *k*<sub>obs,2</sub>, that are obtained from a series of measurements at various temperatures exhibit quite different dependencies on the SDS concentration (Table 3), indicating consecutive rather than parallel reactions, that is:



This conclusion is further supported by the absorption spectra of A, B, and C derived from the global analysis. Taking into account the experimental dead time of the stopped-flow system, the spectrum calculated for A is identical to that of the native state B1[6cLS], whereas for C the Soret band maximum is calculated to be between 400 and 402 nm, which is in good agreement with the experimentally determined Soret band maximum for Cyt-*c* equilibrated in solutions with SDS concentrations > 2 mM. For B, the calculated absorption maximum was found to be at 398 nm, independent of SDS concentration and temperature. Since B and C do not represent pure conformational states but different distributions of B2 species, each of the observed rate constants *k*<sub>obs,*i*</sub> is the sum of individual rate constants that describe the transitions between the various species of Cyt-*c*. The present data agree with previous kinetic measurements using the Trp fluorescence as a probe for the heme pocket structural changes (Das et al. 1998; Gębicka and Gębicki 1999), whereas for the kinetics derived from heme absorption changes a two-fold higher value was reported for the fast phase (Gębicka and Gębicki 1999). This overestimation may result from the less accurate single-wavelength (410 nm) detection mode used by these authors. Conversely, the activation energy derived from fluorescence data (Das et al. 1998) appears to be substantially underestimated (16 kJ/mol) compared to those of the present study (80 and 106 kJ/mol for *k*<sub>obs,1</sub> and *k*<sub>obs,2</sub>, respectively), which in addition compare much better with values derived from unfolding and refolding studies in GuHCl (Elöve et al. 1994; Colón et al. 1997).

## Discussion

The results obtained by various spectroscopic techniques have shown that SDS induces qualitatively different structural changes below and above the CMC. Consequently, these differences are attributed to the different modes of binding by SDS monomers and micelles, i.e. hydrophobic and electrostatic interactions, respectively. Common to both modes of interaction, however, are alterations of the heme structure, implying that sites of electrostatic and hydrophobic attacks should be in the vicinity of the heme pockets.

### Electrostatic and hydrophobic interaction sites

Cyt-*c* exhibits a cationic domain involving seven Lys residues located around the exposed heme edge (Fig. 13) (Bushnell et al. 1990). Owing to this high positive charge density as well as the large molecule dipole moment that points through the center of the ring-like arrangement of the lysines (Koppenol et al. 1991), this protein region constitutes the interaction domain for negatively charged molecules or surfaces, including the binding domains of the natural reaction partners (Pettigrew and Moore 1987; Murgida and Hildebrandt 2001). Hence, this domain is most likely also the preferred interaction site for SDS micelles. As this site is in immediate proximity to the heme, it can readily be understood that electrostatic interactions may perturb the heme pocket structure and eventually lead to the dissociation of the sixth axial ligand from the heme. Note that these structural perturbations are further promoted by external electric fields, as shown for Cyt-*c* electrostatically immobilized on electrodes (Murgida and Hildebrandt 2001).

Owing to its character as a soluble globular protein, Cyt-*c* lacks any extended hydrophobic domains that are exposed to the surface (Bushnell et al. 1990). However, there is a hydrophobic segment in the centre of the ring of lysines that it is located in immediate vicinity of the heme. It is constituted by the amino acids 85 to 81 and thus is directly linked to the axial Met80 ligand of the heme. Upon hydrophobic binding of SDS monomers, this segment may be pulled away from the heme pocket and, hence, cause the rupture of the coordinative

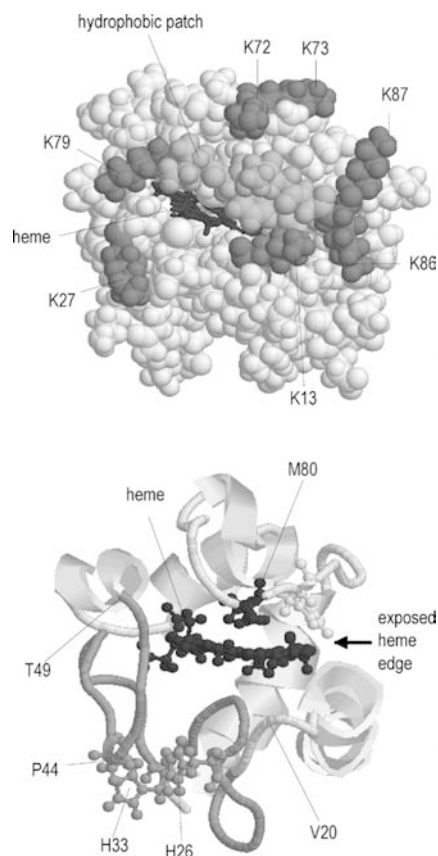


**Fig. 13** Representation of the structure of Cyt-*c* [data taken from the crystal structure (Bushnell et al. 1990)]. *Top*: view of the front surface; *bottom*: view of the peptide segment 20–49

Fe–Met80 bond. A second small hydrophobic segment (43–46) is located more remote from the heme pocket. These hydrophobic patches as well as a few individual hydrophobic amino acids that are directly exposed to the solvent are potentially first targets of hydrophobic attacks by SDS.

#### Binding of SDS monomers and the structural consequences for cytochrome *c*

Upon hydrophobic interactions with SDS monomers, that is below the CMC, far-UV CD spectra reveal a decrease of the  $\alpha$ -helical content by 25%. Most of these secondary structure changes are completed below a SDS concentration of ca. 0.9 mM, which is in line with previous observations (Takeda et al. 1985; Das et al. 1998). At this concentration, ca. 30% of the Cyt-*c* molecules still possess the native Met80 ligand whereas a 90% conversion to the bis-His ligated form B2[6cLS] requires ca. 1.2 mM SDS. Hence, the heme pocket structure changes, which are equally reflected by RR, UV-vis absorption, and Soret-CD spectroscopy, do not parallel the secondary structure changes. These findings suggest that at least a part of the protein structural changes is not related to the formation of the B2 state. In fact, for B2 formed in complexes with phospholipid vesicles, no

alteration of the secondary structure was found (Muga et al. 1991; Heimburg and Marsh 1993). Also, recent kinetic studies indicate that protein and heme structural changes are not fully correlated (Gebicka and Gebicki 1999).

Following this interpretation, the structural changes in the heme pocket are induced by those bound SDS monomers which, as a prerequisite for the ligand exchange, destabilize the front surface of Cyt-*c* via hydrophobic attack on the peptide segment 81–85, as discussed above. As a consequence, the peptide chain from Pro30 (Val20) to Thr49 reorients, such that His33 (His26) is brought in closer proximity to the heme. The formation of B2[6cLS] requires the concerted action of these SDS molecules, denoted as specifically bound monomers, since a 5cHS species that lacks the Met80 ligand but is not yet coordinated by His33 (His26) is not detectable below the CMC. Thus, binding of these SDS molecules may be described according to:

$$K_{\text{sp}} = \frac{[\text{Cyt} - \text{SDS}_N]}{[\text{Cyt}][\text{SDS}]^N} = \frac{[\text{B2}]}{[\text{B1}][\text{SDS}]^N} \quad (5)$$

The concentration of SDS monomers that are not bound to these specific sites is given by:

$$[\text{SDS}] = [\text{SDS}]_{\text{tot}} - N \frac{[\text{B2}]}{[\text{B2}] + [\text{B1}]} \quad (6)$$

where  $[\text{SDS}]_{\text{tot}}$  is the total concentration of SDS. After combination with Eq. (5) one obtains:

$$\log \left( \frac{[\text{B2}]}{[\text{B1}]} \right) = \log K_{\text{sp}} + N \log \left( \frac{[\text{SDS}]_{\text{tot}} - N \frac{[\text{B2}]}{[\text{B2}] + [\text{B1}]}}{[\text{B2}] + [\text{B1}]} \right) \quad (7)$$

which can be fitted to the experimental data, yielding  $N=3.3$ . In an “all-or-none” reaction,  $N$  is the number of those SDS molecules which convert the native Cyt-*c* to the B2[6cLS] state. Since the cooperativity of the process is not infinite,  $N$  can be considered to be the lower limit for the number specifically bound SDS molecules. Equations (5, 6, 7) neglect the binding of SDS molecules that do not lead to the ligand exchange of the heme, which, however, has essentially no impact on the values for  $N$  and  $K_{\text{sp}}$  derived from Eq. 7 in view of the large excess of SDS versus Cyt-*c* in these experiments. Upon increasing the Cyt-*c* concentration to 0.1 mM, as required for low-temperature RR experiments, competitive non-specific SDS binding is not negligible any more and may account for the 10% lower contribution of the B2[6cLS] state determined at the CMC.

#### Binding of SDS micelles and the structural consequences for cytochrome *c*

In solutions containing 50 mM sodium phosphate, interactions with SDS micelles induce the recovery of the secondary structure, as also noted previously (Hirama-

tsu and Yang 1983). These authors attributed this effect to short-range hydrophobic interactions between SDS and the protein matrix, in contrast to mainly long-range hydrophobic interactions between amino acid residues in the native protein structure. A refolding of the protein structure is also observed for Cyt-*c* at low pH by increasing the ionic strength (Goto et al. 1990) or by addition of an anionic fluorescence label (Ali et al. 1999), implying that *electrostatic* interactions promote the formation of a folded and more compact protein structure. This conclusion is in line with the observation by Sanghera and Pinheiro (2000), who demonstrated the recovery of the  $\alpha$ -helical structure when acid-unfolded Cyt-*c* binds to phospholipids micelles.

The secondary structure changes that are induced by SDS micelle binding are accompanied by the formation of HS states B2[5cHS], B2[6cHS(1)], and B2[6cHS(2)], which for the sake of simplicity will be considered in toto and denoted as B2[HS]. Thus, at high SDS concentrations (in 50 mM phosphate buffer) the relative concentration of B2[6cLS] drops to a limiting value of ca. 50%. Again, these findings can be related to the results obtained for binding of acid-unfolded Cyt-*c* to lipid vesicles (Sanghera and Pinheiro 2000). In both cases, the re-folding of the protein does not include the heme pocket since the Soret-CD spectra do not show the characteristic Soret-Cotton effect of the native Cyt-*c*.

Also, binding of micelles can be analysed on the basis of Eqs. (5, 6, 7), assuming that in a micelle/Cyt-*c* complex the ratio of B2[HS] and B2[6cLS] is ca. 1 and the number of SDS molecules in a micelle is 60 (Fig. 7). Then, one obtains  $N=0.75$ , which implies that only one micelle can be bound at the cationic binding domain, as expected on the basis of geometrical considerations.

#### Electrostatic versus hydrophobic interactions

Since both the electrostatic and the hydrophobic interaction domains are located on the front surface of Cyt-*c*, it is very likely that micelle and (specific) monomer binding is competitive. Only in the presence of bound micelles B2[HS] are species formed, implying that this transition requires electrostatic interactions. This conclusion allows understanding of the ionic strength dependence of the conformational changes observed in 20 mM SDS solution (Fig. 9). The increasing ionic strength, which is associated with a decrease of the CMC, causes a lowering of the HS contributions down to 28% at 1 M. At this ionic strength the CMC is ca. 0.3 mM (Emerson and Holtzer 1967), so that the portion of Cyt-*c* loaded with specifically bound SDS molecules cannot exceed 10%. Consequently, the complete conversion of the native Cyt-*c* to the B2 states must largely be due to bound micelles. Thus, the shift of the conformational equilibria from B2[HS] towards B2[6cLS] at high ionic strength reflects a weakening of the electrostatic interactions within the Cyt-*c*/micelle

complex. Note that complex formation itself must be close to 100% even at 1 M ionic strength, since no contributions from the unbound Cyt-*c* can be detected in the RR spectra. In agreement with previous results (Murgida and Hildebrandt 2001; Oellerich et al. 2002), we therefore conclude that electrostatic interactions alone may convert Cyt-*c* into both the B2[6cLS] and the B2[HS] states, whereas the contributions of the latter species increase with the strength of the electrostatic field.

At very low ionic strength in 1 mM HEPES buffer the CMC is estimated to be ca. 7 mM (Emerson and Holtzer 1967). However, it may well be that Cyt-*c* as a poly-electrolyte may lower the CMC so that the increase of the B2[HS] species at SDS concentrations above 4 mM already reflects interactions with SDS micelles (Fig. 8).

The interplay between micelle and monomer binding is more difficult to assess at a Cyt-*c* concentration of 1 mM that had to be employed for NMR and EPR experiments. At such high Cyt-*c* concentrations, protein aggregation is likely to occur, which may affect SDS binding and also the formation of micelles. Nevertheless, the spectral changes observed in the NMR and EPR spectra at SDS concentrations  $\geq 25$  mM can be interpreted on the basis of RR spectroscopic data obtained under the same conditions (spectra not shown). Accordingly, the B2[6cLS] form dominates at 25 mM SDS, whereas the contributions of the B2[HS] forms increase above 50 mM SDS so that the NMR spectral changes can readily be understood. At higher SDS concentrations the relative contributions of the HS species increase, as reflected by the EPR spectra.

#### Conformational dynamics

In freeze-quench experiments the first reaction intermediates that are observed are HS species, including the five-coordinated B2[HS]<sup>fq</sup> and B2[6cHS(1)]; the latter at low temperature undergoes a rapid spin transition and thus is detected as the A[6cLS] state. Within the experimental accuracy, these two species exist in a similar concentration ratio on the entire timescale of the experiments, implying that the interconversion between them is fast. Moreover, also the rise time of these two species could not be resolved properly as the time resolution of the experiments was limited to ca. 20 ms. At this delay time the relative concentrations of B2[HS]<sup>fq</sup> and A[6cLS] is already close to the maximum value that is achieved in the time course of the reaction. Consequently, the true rate constant for the formation of these species,  $k_1$ , may be larger than that obtained by the kinetic simulation. This conclusion is supported by recent kinetic studies based on the detection of the Trp fluorescence (Otzen and Oliveberg 2002).

At the lowest SDS concentration employed (5 mM) the relative concentration of micelles is only ca. 50% of the Cyt-*c* concentration, whereas the concentration of

SDS monomers is higher by a factor of ca. 20. Thus it is reasonable to assume that the formation of the HS species at least partially results from monomer binding, which destabilizes the heme pocket probably via hydrophobic attack on the peptide segment 81–85, the putative primary hydrophobic interaction site. The second step is then attributed to the reorientation of the peptide chain carrying His33 (His26), such that this ligand is brought in proximity to the heme and can form B2[6cLS]. An increase of the SDS concentration above 5 mM corresponds to an increase of the number of micelles in solution. Consequently, the dependence of the rate constants on the SDS concentration reflects the increasing influence of micelle binding. On the basis of our assignments of the electrostatic and hydrophobic binding sites, the increase of  $k_1$  with the SDS micelle concentration can readily be understood since micelle binding also occurs at the front surface of Cyt-*c* and leads to the formation of the HS forms. The subsequent transition from the HS forms to B2[6cLS] ( $k_3$ ), however, is slowed down upon increasing micelle concentration, implying that binding of micelles blocks the access of His33 (His26) to the heme pocket. Consequently,  $k_4$  shows the same SDS dependence since also the release of His33 (His26) from the heme pocket may be hindered by bound micelles. This interpretation is also consistent with the observation that at 150 mM SDS the portion of the initially formed HS state is substantially higher than at low SDS concentration.

The results obtained by stopped-flow experiments can be rationalized in a similar way, although it is not possible to assign the “intermediates” derived from the transient spectra to discrete states of Cyt-*c*. At 2.5 mM SDS the relative concentrations of monomers is ca. 200 times higher than that of micelles, so that binding of monomers is likely to be the origin for the formation of the intermediate “B” which largely represents the HS forms. Micelle binding becomes relevant at higher SDS concentration, as reflected by the increase of  $k_{\text{obs},1}$ . As in the freeze-quench experiments, the subsequent step is attributed to the equilibration with B2[6cLS], which is slowed down with increasing micelle concentration due to blocking of the front surface by bound micelles. The corresponding rate constant  $k_{\text{obs},2}$  exhibits the strongest increase upon raising the temperature, implying that one of the underlying reactions is associated with a large activation energy. This may either be the dissociation of the micelles from the proteins or the movement and reorientation of the peptide chain 30(26)–49. Monitoring the Trp59 fluorescence, stopped-flow measurements of Cyt-*c* binding to lipid vesicles revealed a substantially slower kinetics (Pinheiro et al. 1997; Sanghera and Pinheiro 2000). For the largest fluorescence changes (80–90%), rate constants are determined to be ca.  $0.1 \text{ s}^{-1}$ . Since it is very likely that the environmental changes of Trp59 that give rise to this fluorescence change parallel the heme ligation change, one may conclude that the transition to B2 of Cyt-*c* bound to phospholipids vesicles (Oellerich et al. 2002) is slower by

ca. three orders of magnitude than the SDS-induced B2 formation.

### Mechanism of the conformational conversions

The first event of the structural changes in the heme pocket of Cyt-*c* must be the dissociation of the Met80 ligand from the iron, so it is tempting to identify B2[HS]<sup>fq</sup> as this precursor. The RR spectrum of B2[HS]<sup>fq</sup> indicates a heme pocket structure that differs from that of the B2[5cHS] form observed at equilibrium conditions in complexes with micelles. Thus, it is assumed that B2[HS]<sup>fq</sup> represents a short-lived 5cHS species, which in contrast to B2[5cHS] is not stabilized by appropriate structural changes in the heme pocket. Such structural changes do not occur even on the timescale of seconds, implying that the formation of B2[5cHS] follows that of B2[6cLS], which proceeds on the long millisecond timescale. Also the B2[6cHS(2)] state cannot be detected on the timescale of the freeze-quench experiments. The formation of this state is likely to occur on an even longer timescale since it requires more extended structural changes inasmuch as also the His18 ligand is removed from the heme (Oellerich et al. 2002).

The Cyt-*c* states formed by interaction with SDS exhibit the same ligation pattern as some of the species formed during GuHCl-induced unfolding of the protein (Oellerich et al. 2002) and in both cases the bis-His ligated 6cLS form represents a relatively stable state (kinetic trap) on the unfolding and refolding pathways (cf. Colón et al. 1997; Yeh et al. 1997, 1998, and references therein). Furthermore, the first steps of the structural changes induced by SDS or GuHCl, that is, the dissociation of the native Met80 ligand from the heme and the subsequent binding of a water molecule, occur on the submillisecond and short millisecond timescales, respectively, as inferred from the present and previous data (Yeh et al. 1998; Otzen and Oliveberg 2002). Within the framework of the present interpretation, these structural changes exclusively originate from an electrostatic or hydrophobic attack on the front surface of the protein. For these transitions, major structural changes of the polypeptide chain are not required, which in fact are quite different in the SDS and GuHCl systems (cf. Oellerich et al. 2002). The subsequent formation of the bis-His coordinated 6cLS state follows a movement of a large peptide segment and, hence, is expected to differ in SDS and GuHCl such that kinetic data are hard to compare. Nevertheless, it appears to be that in neutral solutions the SDS-induced formation of B2[6cLS] is substantially faster than the corresponding transition in GuHCl (Table 2; Elöve et al. 1994). Conversely, there is a substantial acceleration of the structural changes in the heme pocket in GuHCl at low pH, which is evidently associated with the far-reaching unfolding of the polypeptide chain (Elöve et al. 1994; Yeh et al. 1998). Thus, the mobility of peptide segments and the accessibility of

the heme for His33 (His26) are less restricted than upon interaction with SDS. On the other hand, the conformational changes in the heme pocket are much slower upon binding to phospholipids vesicles (Pinheiro et al. 1997; Sanghera and Pinheiro 2000). It may be that hydrophobic interactions with SDS monomers accelerate the conformational transition to B2. Alternatively, or additionally, the Cyt-*c*/vesicle complex that is formed in the first step of the reaction is more stable than the Cyt-*c*/micelle complex such that the subsequent protein structural changes on the pathway to B2[6cLS] are kinetically blocked.

### Structural changes under physiological conditions

The front surface of Cyt-*c* that has been assigned to be the site for specific binding SDS monomers and micelles also represents the domain for interacting with CcO (Pettigrew and Moore 1987; Ferguson-Miller and Babcock 1996; Roberts and Pique 1999). Thus, both electrostatic and hydrophobic interactions are involved in forming the Cyt-*c*/CcO complex such that the essential requirements for inducing a conformational transition to state B2 are fulfilled. In fact, this transition has been shown to occur in the fully oxidized Cyt-*c*/CcO complex under stationary conditions at low ionic strength (ca. 15 mM) (Döpner et al. 1999). Under physiological conditions the ionic strength is ca. 10 times higher, so that electrostatic interactions may be weakened and the lifetime of the complex is in the short millisecond range (Soulimane and Buse 1995; Wackerbarth et al. 2001). The formation of the states B2[6cLS] and B2[5cHS], however, occurs much slower, at least upon binding to SDS. Conversely, the rise time of the precursor of this conformational transition, B2[HS]<sup>fq</sup>, is faster than 20 ms, indicating that the dissociation of the Met80 ligand from the heme may well proceed on a timescale similar to the lifetime of the physiological Cyt-*c*/CcO complex. The driving force of the intermolecular electron transfer from the reduced state B1 to the Cu<sub>A</sub> centre of CcO is ca. 0 eV (Malatesta et al. 1995), such that forward and back reactions occur with essentially the same rate of ca. 10<sup>5</sup> s<sup>-1</sup>. Unidirectionality of the enzymatic process is thought to be achieved by the subsequent intramolecular electron transfer steps in CcO, which, however, are slower by at least one order of magnitude (Geren et al. 1995). On the other hand, rupture of the Met80–Fe bond in the protein complex would prevent unproductive back electron transfer from CcO to Cyt-*c* due to a negative shift of the redox potential, which is likely to be similar to that of B2[5cHS] (Hildebrandt and Stockburger 1989a, 1989b; Wackerbarth et al. 2001). Thus, ligand dissociation could be essential for the efficiency of the enzymatic process. This conclusion is supported by previous findings that the enzymatic activity of CcO versus Cyt-*c* variants determined in steady-state kinetic experiments correlates with the portion of B2 formed in the fully oxidized protein

complexes (Döpner et al. 1999). In fact, the present freeze-quench experiments have shown that the equilibrium concentration of B2 is related to the intermediary concentration of B2[HS]<sup>fq</sup>.

First evidence for structural changes of Cyt-*c* in the apoptotic reaction cascade was provided by Jemmerson et al. (1999), who found that antibodies recognizing apoptotic Cyt-*c* also complex the membrane-bound but not the native protein. These results already suggest that the structure of apoptotic Cyt-*c* is closely related to that of state B2 as this is the prevailing form in complexes with phospholipid vesicles (Döpner et al. 1999; Oellerich et al. 2002). Further support for this conclusion is based on the observation that these antibodies specifically interact with the region around Pro44 (Jemmerson et al. 1999). This part of the protein surface will necessarily be altered upon rearranging the peptide segment 30(20)–49 to allow His33 (His26) to bind to the heme. Since this B2[6cLS] state is preferentially formed in the ferric state (Rivas et al. 2002), this interpretation is consistent with the conclusion that only the oxidized protein is involved in apoptosis (Hancock et al. 2001).

Apoptotic Cyt-*c* forms a complex with Apaf-1 with a binding constant that is higher by several orders of magnitude than that for the Cyt-*c*/CcO complex (Purring et al. 1999). Whereas in the latter case a tight binding would oppose a fast enzymatic turnover, complex formation with Apaf-1 must obviously be irreversible for Cyt-*c*'s function in apoptosis. Thus, the structural changes of apoptotic Cyt-*c* do not have to proceed very fast but the resultant state must represent a relatively stable form. This conclusion is consistent with the assignment of apoptotic Cyt-*c* to state B2 in which the protein structural changes required for His33 (His26) coordination have taken place. The kind of interactions in the Cyt-*c*/Apaf-1 complex appears to be predominantly electrostatic (Purring-Koch and McLendon 2000). However, the amino acids of Cyt-*c* that have been identified to be involved in complex formation are not restricted to lysine residues on the front surface but are also located on the opposite side of the protein. Even though the formation of B2 includes a rearrangement of a part of the protein surface, the interaction domain in the complex with Apaf-1 must be much more extended than for binding to CcO, which has been interpreted in terms of a partial encapsulation in the WD-40 domain of Apaf-1 (Yu et al. 2001). In such a complex, the mobility of peptide segments should be more restricted than for Cyt-*c* bound to the surface of SDS micelles. Thus, it may be that under physiological conditions the conformational changes of apoptotic Cyt-*c* precede binding to Apaf-1, as suggested by Jemmerson et al. (1999). Specifically, the formation of B2 may be the prerequisite for or induced during the transfer across the mitochondrial membrane. In fact, the transition to B2 is strongly promoted upon (partial) penetration into the hydrophobic regions of model membranes (Rivas et al. 2002) or upon hydrophobic binding of only a few amphipathic molecules. This latter case is not restricted to the SDS

studied in this work but may also hold for binding of fatty acids (Stewart et al. 2000), which have in fact been implicated to cause apoptosis via inducing Cyt-*c* release to the cytosol (Di Paola et al 2000).

## Conclusions

1. SDS monomers and micelles bind to Cyt-*c* via hydrophobic and electrostatic interactions, respectively. In both cases, the specific binding domains are most likely located on the front surface of the protein close to the exposed heme edge.
2. The structural consequences of hydrophobic and electrostatic SDS binding include the dissociation of the Met80 ligand from the heme and the reorientation of a major peptide segment to enable ligation by His33 (His26). In the case of electrostatic interactions, the coordinative His33 (His26)–Fe bond may be weakened such that high-spin species are stabilized.
3. Further structural changes of the protein matrix specifically induced by interactions with SDS monomers do not parallel the heme pocket structural changes and may occur remote from the specific binding domain.
4. The formation of B2 occurs on the long millisecond timescale. A precursor that lacks the Met80 ligand but still seems to possess the overall structure of the native protein is formed in the short millisecond range or even faster.
5. Dissociation of Met80 from the heme of ferric Cyt-*c* may be involved in the physiological redox process with CcO and prevent unproductive back electron transfer. The relatively stable conformational state B2 is suggested to be the physiologically active species in apoptosis and may be formed either upon binding to Apaf-1 or before, during the release of Cyt-*c* into the cytosol.

**Acknowledgements** The authors thank Dr. E. Bill, Prof. N. Metzler-Nolte, and Dr. R. Schumacher for kind support in EPR, NMR, and stopped-flow experiments, respectively. Technical assistance by B. Deckers is gratefully acknowledged. The work was supported by the Volkswagen-Stiftung (I 72826).

## References

Alden RG, Crawford BA, Doolen R, Ondrias MR, Shelnutt JA (1989) Ruffling of nickel(II)-octaethylporphyrin in solution. *J Am Chem Soc* 111:2070–2072

Ali V, Prakash K, Kulkarni S, Ahmad A, Madhusudan KP, Bhakuni V (1999) 8-Anilino-1-naphthalenesulfonic acid (ANS) induces folding of acid unfolded cytochrome *c* to molten globule state as a result of electrostatic interactions. *Biochemistry* 38:13635–13642

Bushnell GW, Louie GV, Brayer GD (1990) High-resolution three-dimensional structure of horse heart cytochrome *c*. *J Mol Biol* 214:585–595

Cartling B (1983) Intermediate and stable redox states of cytochrome *c* studied by low-temperature resonance Raman spectroscopy. *Biophys J* 43:191–205

Colón W, Wakem LP, Sherman F, Roder H (1997) Identification of the predominant non-native histidine ligand in unfolded cytochrome *c*. *Biochemistry* 36:12535–12541

Das TK, Mazumdar S, Mitra S (1998) Characterization of a partially unfolded structure of cytochrome *c* induced by sodium dodecyl sulphate and the kinetics of its refolding. *Eur J Biochem* 254:662–670

Davies AM, Guillemette JG, Smith M, Greenwood C, Thurgood AGP, Mauk AG, Moore GR (1993) Redesign of the interior hydrophilic region of mitochondrial cytochrome *c* by site-directed mutagenesis. *Biochemistry* 32:5431–5435

de Jongh HHJ, Killian JA, de Kruijff B (1992) A water-lipid interface induces a highly dynamic folded state in apocytochrome *c* and cytochrome *c*, which may represent a common folding intermediate. *Biochemistry* 31:1636–1643

Di Paola M, Cocco T, Lorusso M (2000) Arachidonic acid causes cytochrome *c* release from heart mitochondria. *Biochem Biophys Res Commun* 277:128–133

Döpner S, Hildebrandt P, Mauk AG, Lenk H, Stempfle W (1996) Analysis of vibrational spectra of multicomponent systems. Application to pH-dependent resonance Raman spectra of ferricytochrome *c*. *Spectrochim Acta, Part A* 52:573–584

Döpner S, Hildebrandt P, Rosell FI, Mauk AG, von Walter M, Buse G, Soulimane T (1999) The structural and functional role of lysine residues in the binding domain of cytochrome *c* in the electron transfer to cytochrome *c* oxidase. *Eur J Biochem* 261:379–391

Elöve GA, Bhuyan AK, Roder H (1994) Kinetic mechanism of cytochrome *c* folding: involvement of the heme and its ligands. *Biochemistry* 33:6925–6935

Emerson MF, Holtzer A (1967) On the ionic strength dependence of micelle number. *J Phys Chem* 71:1898–1907

Ferguson-Miller S, Babcock GT (1996) Heme/copper terminal oxidases. *Chem Rev* 96:2889–2907

Gębicka L, Gębicki JL (1999) Kinetic studies on the interaction of ferricytochrome *c* with anionic surfactants. *J Protein Chem* 18:165–172

Geren LM, Beasley JR, Fine BR, Saunders AJ, Hibdon S, Pielak GJ, Durham B, Millett F (1995) Design of a ruthenium cytochrome *c* derivative to measure electron transfer to the initial acceptor in cytochrome *c* oxidase. *J Biol Chem* 270:2466–2472

Goto Y, Calciano LJ, Fink AL (1990) Acid-induced folding of proteins. *Proc Natl Acad Sci USA* 87:573–577

Hancock JT, Desikan R, Neill SJ (2001) Does the redox status of cytochrome *c* act as a fail-safe mechanism in the regulation of programmed cell death? *Free Radical Biol Med* 31:697–703

Heimburg T, Marsh D (1993) Investigation of secondary and tertiary structural changes of cytochrome *c* in complexes with anionic lipids using amide hydrogen exchange measurements: an FTIR study. *Biophys J* 65:2408–2417

Hildebrandt P, Stockburger M (1989a) Cytochrome *c* at charged interfaces. 1. Conformational and redox equilibria at the electrode electrolyte interface probed by surface-enhanced resonance Raman spectroscopy. *Biochemistry* 28:6710–6721

Hildebrandt P, Stockburger M (1989b) Cytochrome *c* at charged interfaces. 2. Complexes with negatively charged macromolecular systems studied by resonance Raman spectroscopy. *Biochemistry* 28:6722–6728

Hildebrandt P, Heimburg T, Marsh D (1990) Quantitative conformational analysis of cytochrome *c* bound to phospholipid vesicles studied by resonance Raman spectroscopy. *Eur Biophys J* 18:193–201

Hiramatsu K, Yang JT (1983) Cooperative binding of hexadecyltrimethylammonium chloride and sodium dodecyl sulfate to cytochrome *c* and the resultant change in protein conformation. *Biochim Biophys Acta* 743:106–114

Jemmerson R, Liu J, Hausauer D, Lam KP, Mondino A, Nelson RD (1999) A conformational change in cytochrome *c* of apoptotic and necrotic cells is detected by monoclonal antibody

- binding and mimicked by association of the native antigen with synthetic phospholipid vesicles. *Biochemistry* 38:3599–3609
- Kitagawa T, Ozaki Y (1987) Infrared and Raman spectra of metalloporphyrins. *Struct Bonding* 64:73–114
- Koppenol WH, Rush JD, Mills JD, Margoliash E (1991) The dipole moment of cytochrome *c*. *Mol Biol Evol* 8:545–558
- Makinen MW, Churg AK (1983) Structural and analytical aspects of the electronic spectra of heme proteins. In: Lever ABP, Gray HB (eds) *Iron porphyrins*. Addison-Wesley, Reading, Mass., USA, pp 141–219
- Malatesta F, Antonini G, Sarti P, Brunori M (1995) Structure and function of a molecular machine: cytochrome *c* oxidase. *Biophys Chem* 54:1–33
- Muga A, Mantsch HH, Surewicz WK (1991) Membrane binding induces destabilization of cytochrome *c* structure. *Biochemistry* 30:7219–7224
- Murgida DH, Hildebrandt P (2001) Heterogeneous electron transfer of cytochrome *c* on coated silver electrodes. Electric field effects on structure and redox potentials. *J Phys Chem B* 105:1578–1586
- Oellerich S (2001) PhD thesis. MPI für Strahlenchemie Mülheim/University of Essen
- Oellerich S, Bill E, Hildebrandt P (2000) Freeze-quench resonance Raman and electron paramagnetic resonance spectroscopy for studying enzyme kinetics: application to azide binding to myoglobin. *Appl Spectrosc* 54:1480–1484
- Oellerich S, Wackerbarth H, Hildebrandt P (2002) Spectroscopic characterization of non-native conformational states of cytochrome *c*. *J Phys Chem B* 106:6566–6580
- Otzen DE, Oliveberg M (2002) Burst phase expansion of the native protein prior to global unfolding in SDS. *J Mol Biol* 315:1231–1240
- Parthasarathi N, Hansen C, Yamaguchi S, Spiro TG (1987) Metalloporphyrin core size resonance Raman marker bands revisited: implications for the interpretation of hemoglobin photoproduct Raman frequencies. *J Am Chem Soc* 109:3865–3871
- Pettigrew GW, Moore GR (1987) *Cytochromes c: biological aspects*. Springer, Berlin Heidelberg New York
- Pinheiro TJT (1994) The interaction of horse heart cytochrome *c* with phospholipid bilayers: structural and dynamic effects. *Biochimie* 76:489–500
- Pinheiro TJT, Elöve GA, Watts A, Roder H (1997) Structural and kinetic description of cytochrome *c* unfolding induced by the interaction with lipid vesicles. *Biochemistry* 36:13122–13132
- Purring-Koch C, McLendon G (2000) Cytochrome *c* binding to Apaf-1: the effects of dATP and ionic strength. *Proc Natl Acad Sci USA* 97:11923–11931
- Purring C, Zou H, Wang X, McLendon G (1999) Stoichiometry, free energy, and kinetic aspects of cytochrome *c*: Apaf-1 binding in apoptosis. *J Am Chem Soc* 121:7435–7436
- Reynolds JA, Tanford C (1970) Binding of dodecyl sulfate to proteins at high binding ratios. Possible implications for the state of proteins in biological membranes. *Proc Natl Acad Sci USA* 66:1002–1007
- Rivas L, Murgida DH, Hildebrandt P (2002) Conformational and redox equilibria and dynamics of cytochrome *c* immobilized on electrodes via hydrophobic interactions. *J Phys Chem B* 106:4823–4830
- Roberts VA, Pique ME (1999) Definition of the interaction domain for cytochrome *c* on cytochrome *c* oxidase. III. Prediction of the docked complex by a complete, systematic search. *J Biol Chem* 274:38051–38060
- Sanghera N, Pinheiro TJT (2000) Unfolding and refolding of cytochrome *c* driven by the interaction with lipid micelles. *Protein Sci* 9:1194–1202
- Scott RA, Mauk AG (1996) *Cytochrome c: a multidisciplinary approach*. University Science Books, Sausalito, Calif., USA
- Shi YG (2001) A structural view of mitochondria-mediated apoptosis. *Nat Struct Biol* 8: 394–401
- Smith WE (1993) Surface enhanced resonance Raman spectroscopy. *Methods Enzymol* 226C:482–495
- Soulimane T, Buse G (1995) Integral cytochrome *c* oxidase: preparation and progress towards a 3-dimensional crystallization. *Eur J Biochem* 227:588–595
- Spooner PJR, Watts A (1991) Reversible unfolding of cytochrome *c* upon interaction with cardiolipin bilayers. I. Evidence from deuterium NMR measurements. *Biochemistry* 30:3871–3879
- Stewart JM, Blakely JA, Johnson MD (2000) The interaction of ferrocycytochrome *c* with long-chain fatty acids and their CoA and carnitine esters. *Biochem Cell Biol* 78:675–681
- Takeda K, Takahashi K, Batra PP (1985) Kinetic aspects of the interaction of horse heart cytochrome *c* with sodium dodecyl sulfate. *Arch Biochem Biophys* 236:411–417
- Wackerbarth H, Klar U, Gunther W, Hildebrandt P (1999) Novel time-resolved surface-enhanced (resonance) Raman spectroscopic technique for studying the dynamics of interfacial processes: application to the electron transfer reaction of cytochrome *c* at a silver electrode. *Appl Spectrosc* 53:283–291
- Wackerbarth H, Murgida DH, Oellerich S, Döpner S, Rivas L, Hildebrandt P (2001) Dynamics and mechanism of the electron transfer process of cytochrome *c* probed by resonance Raman and surface enhanced resonance Raman spectroscopy. *J Mol Struct* 563:51–59
- Witt H, Malatesta F, Nicoletti F, Brunori M, Ludwig B (1998) Tryptophan 121 of subunit II is the electron entry site to cytochrome-*c* oxidase in *Paracoccus denitrificans*: involvement of a hydrophobic patch in the docking reaction. *Eur J Biochem* 251:367–373
- Yeh SR, Takahashi S, Fan BC, Rousseau DL (1997) Ligand exchange during cytochrome *c* folding. *Nat Struct Biol* 4:51–56
- Yeh SR, Han SW, Rousseau DL (1998) Cytochrome *c* folding and unfolding: a biphasic mechanism. *Acc Chem Res* 31:727–736
- Yoshimura T (1988) A change in the heme stereochemistry of cytochrome *c* upon addition of sodium dodecylsulfate: electron paramagnetic resonance and electronic absorption spectral study. *Arch Biochem Biophys* 264:450–461
- Yu TN, Wang XD, Purring-Koch C, Wei Y, McLendon GL (2001) A mutational epitope for cytochrome *c* binding to the apoptosis protease activation factor-1. *J Biol Chem* 276:13084–13088